Hindawi
International Journal of Antennas and Propagation
Volume 2023, Article ID 9769872, 1 page
https://doi.org/10.1155/2023/9769872

Retraction

Retracted: Research on Quantization Error Influence of Millimeter-Wave Phased Array Antenna

International Journal of Antennas and Propagation

Received 19 December 2023; Accepted 19 December 2023; Published 20 December 2023

This article has been retracted by Hindawi following an investigation undertaken by the publisher [1]. This investigation has uncovered evidence of one or more of the following indicators of systematic manipulation of the publication process:

(1) Discrepancies in scope
(2) Discrepancies in the description of the research reported
(3) Discrepancies between the availability of data and the research described
(4) Inappropriate citations
(5) Incoherent, meaningless and/or irrelevant content included in the article
(6) Manipulated or compromised peer review

The presence of these indicators undermines our confidence in the integrity of the article's content and we cannot, therefore, vouch for its reliability. Please note that this notice is intended solely to alert readers that the content of this article is unreliable. We have not investigated whether authors were aware of or involved in the systematic manipulation of the publication process.

Wiley and Hindawi regrets that the usual quality checks did not identify these issues before publication and have since put additional measures in place to safeguard research integrity.

We wish to credit our own Research Integrity and Research Publishing teams and anonymous and named external researchers and research integrity experts for contributing to this investigation.

The corresponding author, as the representative of all authors, has been given the opportunity to register their agreement or disagreement to this retraction. We have kept a record of any response received.

References

[1] H. Yang, L. Zhu, Z. Xia et al., "Research on Quantization Error Influence of Millimeter-Wave Phased Array Antenna," *International Journal of Antennas and Propagation*, vol. 2021, Article ID 1874537, 19 pages, 2021.

Hindawi
International Journal of Antennas and Propagation
Volume 2021, Article ID 1874537, 19 pages
https://doi.org/10.1155/2021/1874537

Research Article

Research on Quantization Error Influence of Millimeter-Wave Phased Array Antenna

Haigen Yang,[1] Linqun Zhu,[1] Zhun Xia,[1] Yanqing Chen,[1] Luohao Dai,[1] Ruotian Xu,[1] YuanHao Chen,[1] Luyang Li,[1] GuiYing Sun,[2] Hongyang Yu,[3] and Wenting Xu[3]

[1]*Engineering Research Center of Wider and Wireless Communication Technology of Ministry of Education, Nanjing University of Posts and Telecommunications, Nanjing 21003, China*
[2]*Chinese People's Liberation Army, No. 61416, Beijing 100089, China*
[3]*Beijing Electro-Mechanical Engineering Institute, Beijing 100074, China*

Correspondence should be addressed to Haigen Yang; yhg@njupt.edu.cn

Received 24 July 2021; Revised 23 August 2021; Accepted 13 September 2021; Published 25 September 2021

Academic Editor: Fangqing Wen

The millimeter-wave phased array antenna is a higher integration system that is composed of different subarray modules, and in actual engineering, the existing amplitude, phase errors, and structural errors will change the performance of the array antenna. This paper studies the influence of the random amplitude and phase errors of the antenna array in the actual assembly process and the actual position errors between the subarrays on the electrical performance of the antenna. Based on the planar rectangular antenna array-electromagnetic coupling model, we propose a method of verifying the effect of random errors on the phased array antenna. The simulation result shows that the method could obtain the critical value of the error generated by the antenna subarray during processing and assembly. To reduce the error factor, it is necessary to ensure that the random phase and amplitude error should not exceed $(10^\circ, 0.5\,\text{dB})$. The error in the X-direction during assembly should be $\leq 0.05\lambda$, and the error in the Y-direction should be $\leq 0.1\lambda$. When symmetrical deformation occurs, the maximum deformation should be less than 0.05λ.

1. Introduction

The antenna is an important part of radar, and the advancement of radar technology is inseparable from reliable and stable radar signals, which will directly affect the detection effect of radar [1]. However, the directivity of a single antenna is limited, to use antennas for electrical scanning in space, several antennas can be arranged together regularly to produce a directional pattern, which is called an antenna array [2]. The millimeter wave has a short wavelength and has the comprehensive advantages of microwave and light waves. The antenna array using millimeter wave has the advantages of extremely wide bandwidth, small size, compact system structure, and electromagnetic energy focusing [3], which is especially suitable for radar and other equipment.

Driven by the rapid development of mobile communication systems, in order to better apply this multi-antenna array element structure to radar equipment, phased array systems and multiple input multiple output (MIMO) systems have emerged. Among them, the phased array system has been widely used on ground radars as early as the 1850s, and the MIMO concept was first introduced into radar technology in 2004, mainly using beam diversity to analyze and study the angle of arrival of the signal. Although the theories are similar, the application scenarios are quite different. MIMO radar is mostly used in civilian applications, such as the Industrial Internet of Things (IoT), due to its high packet loss rate and decreased multiplexing gain in high-speed conditions, and it is used in conjunction with the 5G technology being deployed to meet the needs of industrial communication systems [4]. In order to improve its performance, the model and algorithm need to be continuously improved. The so-called quaternion noncircular MUSIC (QNC-MUSIC) algorithm was proposed to improve the accuracy of DOA estimation in [5]. Shi et al. constructed a generalized tensor model in [6] and optimized the tensor by maximizing the number of detection targets, and finally derived the Cramér–Rao Bound (CRB) of nested radars, which proves the superiority of the method. A bistatic coprime EMVS-MIMO radar framework was proposed in [7], and the work in [8] proposed a new closed-form estimation algorithm for EMVS-MIMO radar, constructed a new rotation invariant characteristic, and achieved better estimation than existing algorithms.

Compared with MIMO radar, phased array radar has a huge cost, larger volume and weight, a long history of development, and relatively complete technology, and it is mostly used in large-scale shipborne and airborne radars [9]. The antenna element spacing at the transmitting end of a phased array radar is usually on the order of wavelength. In order to prevent grating lobes from appearing, the spacing is usually set to half a wavelength. In MIMO radar, the sensor spacing should not exceed half a wavelength to avoid phase ambiguity [10]. Compared with conventional arrays, active phased array antennas have the advantages of multifunction, high reliability, and high detection and tracking capabilities [11]. Vollbracht determined the optimal phase excitation distribution through the study of the single-feed antenna array, and it was confirmed on the 4×8 antenna subarray [12]. Sharma also proposed a new phased array composed of antijamming antennas [13]. Recently, a highly efficient polarized 8×8 millimeter-wave antenna array in the 60 GHz frequency band was proposed in [14]. Compared with the traditional array, its impedance bandwidth, stable gain, and radiation within the bandwidth are improved. Ortiz et al. used a mathematical model based on diffraction theory to evaluate the influence of mutual coupling between polarized antennas [15].

Conventional phased array antennas have problems such as greater complexity and high cost [16]; we can use digital technologies splice digital array unit formed of different sizes and form fronts to reduce design difficulty [17]. However, in practical engineering, there are extensive excitation errors caused by amplitude and phase changes [18], as well as deformation errors caused by processing and using. Therefore, in order to achieve the expected antenna sidelobe requirements and obtain a stable array design, it is necessary to perform error analysis on the assembled antenna array [19]. Wang analyzed the influence of random feeding errors such as the failure rate of the array element and the feeding amplitude and phase error on the electrical performance of the phased array antenna, which analyzed the bowl surface deformation and bending deformation of both systematic errors impact the electrical properties of a phased array antenna [20]. Chen and Zhou proposed a mathematical model of the thermal deformation error of the active phased array to analyze the influence of such errors on the antenna pattern [21].

The current research on the performance of phased array radar mainly focuses on the influence of various factors on the electrical performance of the antenna when the radar is used, and the errors caused by the production process and assembly accuracy are often ignored. This article is mainly based on the error theory modeling of the millimeter-wave array antenna. The model is composed of two 16×8 rectangular subarrays and works in the 24.25 GHz~27.5 GHz frequency band. Based on the array antenna algorithm of this model, we can introduce random amplitude and phase errors of each channel and structural errors caused by array deformation [22]. Observe its influence on the performance of antenna gain, sidelobe level, beam width, etc. [23–25], realize the rapid analysis of the influence of the two types of errors on the electrical performance of the antenna array, establish the interval model of the relevant input parameters, and give the fluctuation interval of the relevant index, to provide support for the robust design of the millimeter-wave phased array antenna array.

2. Research of Active Phased Array Antennas

As a special type of antenna, the phased array antenna is composed of many identical independent antenna elements to form an antenna array. By controlling the radiation energy and phase relationship between each unit and using different array arrangements for each antenna unit in the array, the excitation feedback relationship affects the radiation field of the entire array, and accurate and predictable radiation patterns and beam directions are obtained, to improve the gain, scanning frequency, and anti-interference of the array [26].

Compared with the traditional passive array, the active array adopts a distributed feedback structure, that is, each unit in the antenna array has a complete transmit/receive (T/R) unit to achieve high-power amplification and high-sensitivity reception [27]. Compared with other arrays, the active phased array has flexibility in beam direction, can form and independently control multiple beams, and search, identify, and track multiple targets. At the same time, because the active phased array antenna adopts millimeter wave with high power, its anti-interference ability is greatly increased [28].

Phased array antennas are usually divided into two types: linear array and area array. The linear array only has one-dimensional scanning capability. If you want to have two-dimensional scanning capability, you need to combine multiple one-dimensional linear arrays to form a planar array antenna.

Figure 1 shows a rectangle of $M \times N$ antenna elements of the grid planar array antenna; the center position of the antenna element is $r_{m,n} = \hat{x} m d_x + \hat{y} n d_y$. Assuming that the antenna element patterns are the same, and the analysis method is similar to a linear array, the array factor of the planar array antenna can be obtained as

$$F(\theta, \phi) = \sum_{m,n} \left| a_{m,n} \right| \exp\left\{ jk \left[m d_x (u - u_0) + n d_y (v - v_0) \right] \right\}, \tag{1}$$

where $u = \sin\theta\cos\phi$, $v = \sin\theta\sin\phi$, $u_0 = \sin\theta_0\cos\phi_0$, and $v_0 = \sin\,\theta_0 \sin\,\phi_0$. The pencil beam is a typical feature of the planar antenna array pattern. When the excitation amplitude of each antenna element is equal, a uniform planar

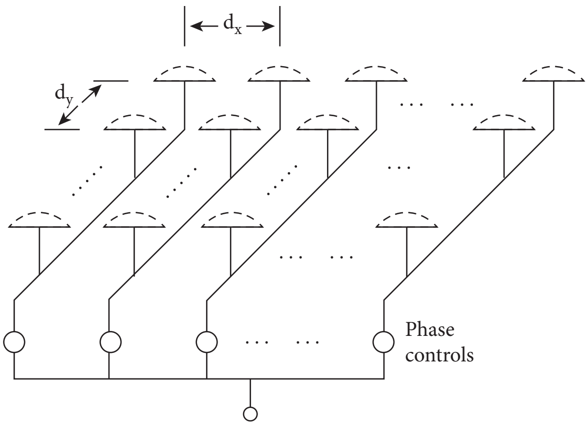

Figure 1: Planar array antenna diagram [29].

array is obtained. Normalize the above formula to get the matrix factor of the uniform plane array:

$$F(\theta,\phi)=\frac{\sin\left[M\pi d_x(u-u_0)/\lambda\right]}{M\sin\left[\pi d_x(u-u_0)/\lambda\right]}+\frac{\sin\left[N\pi d_y(v-v_0)/\lambda\right]}{N\sin\left[\pi d_y(v-v_0)/\lambda\right]}. \tag{2}$$

3. Error Modeling Theory

In the actual design process, the influence of various errors on the active phased array antenna must be considered. These errors have both random errors and systematic errors, which may be caused by component defects, or they may be caused by the feeder network, or other factors. These errors may cause the antenna gain to decrease, the sidelobe level to increase, the beam width to expand, the radiation efficiency to decrease, and even affect the antenna's beam pointing, which largely determines the performance of active phased array radar [30]. The errors mentioned above are all random errors, which cannot be eliminated due to their contingency and unpredictability, and the performance of all large antenna arrays is affected by random errors such as element position and amplitude and phase changes [31].

3.1. Planar Array Antenna Modeling. In order to facilitate the simulation calculation of the two-dimensional phased array antenna pattern, using the coordinate system is usually chosen to express the direction in the simulation. In order to facilitate multidimensional process analysis and experimental verification, the representation method adopted is as follows: the two-dimensional pattern is represented by the antenna coordinate system, and the three-dimensional pattern is represented by the sinusoidal coordinate system [32].

This article revolves around two-dimensional array pattern modeling. In the antenna coordinate system, the coordinate of R can be characterized by the parameter θ and the parameter ϕ. Among them, θ is the angle from the z-axis to the point $R(0^0\le\theta\le180^0)$, ϕ, and ϕ is the angle between the x-axis and the projection line of R on the XY-plane. Normalize the amplitude of R, and the coordinate value corresponding to R_0 is $(\sin\theta\cos\phi, \sin\theta\sin\phi, \cos\theta)$. The antenna coordinate system of the array direction diagram is shown in Figure 2.

The sine space is a hemispherical mapping from a three-dimensional space to a two-dimensional plane, represented by three variables U, V, and W, which can more intuitively characterize the antenna coordinate system. The transformation formula from antenna coordinate system to sine space is as follows:

$$\begin{aligned}U&=\sin\theta\cos\phi,\\V&=\sin\theta\sin\phi,\\W&=\cos\theta.\end{aligned} \tag{3}$$

For the visible space of a two-dimensional planar phased array antenna, the value range of U and V is $[-1,1]$, and the value range of W is $[0,1]$. For an ideal planar array, there is no z-component in the position function of the array element, so there is no need to consider the influence of W on the array.

Assuming the two-dimensional planar phased array has $M\times N$ radiation channels [33], the rectangular grid arrangement, the channel spacing is d_x and d_y, respectively, the phase center position of the radiation unit is $r_{m,n}=\hat{x}md_x+\hat{y}nd_y$. The array arrangement can be seen in Figure 1.

Then, the array factor pattern of the planar array antenna is

$$AF=\sum_{m,n}^{M,N}A_{mn}\exp\left[jk\left(md_xu+nd_yv\right)\right],\quad k=\frac{2\pi}{\lambda}. \tag{4}$$

Among them, M and N, respectively, represent the number of azimuth and elevation dimensions of the planar phased array antenna, and u and v, respectively, represent the coordinates of the UV-plane in the sine space representation, where the corresponding point of the incident angle is located, $u=\sin\theta\cos\phi$, $v=\sin\theta\sin\phi$. θ and ϕ are two parameters representing the spatial angle in the antenna coordinate system; A_{mn} is the complex excitation signal of radiation channels (m, n):

$$\begin{aligned}A_{mn}&=I_{mn}\exp\left(-jk\left(md_xu_0+nd_yv_0\right)\right),\\u_0&=\sin\theta_0\cos\phi_0,\\v_0&=\sin\theta_0\sin\phi_0.\end{aligned} \tag{5}$$

I_{mn} is the weighted amplitude of radiation channels (m, n), and (θ_0,φ_0) is the beam direction of the antenna. Then, the pattern of the two-dimensional array antenna can be expressed as

$$AF=\sum_{m,n}I_{mn}\exp\left\{jk\left[md_x(u-u_0)+nd_y(v-v_0)\right]\right\}. \tag{6}$$

According to the principle of pattern product, considering the influence of the element pattern on the array pattern, the expression of the two-dimensional array antenna can be expressed as

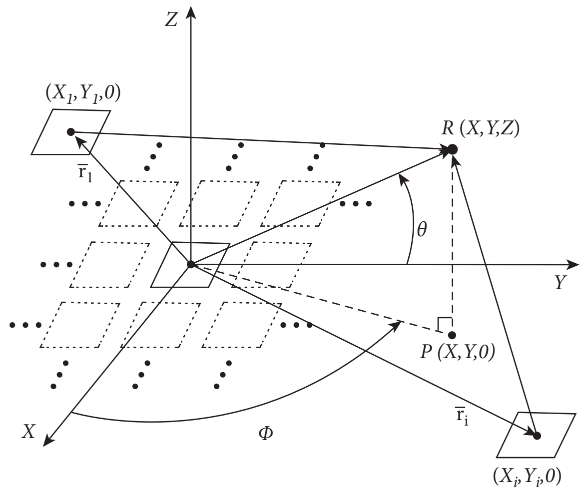

FIGURE 2: Antenna coordinate system [29].

$$E(\theta,\phi) = EP * AF = f(\theta,\phi) * AF, \tag{7}$$

where $EP = f(\theta,\phi)$ is the pattern of the antenna elements in the array.

3.2. Random Error of Amplitude and Phase. In actual engineering, there will be some errors in the amplitude and phase of the array element. Assume that the amplitude error of array element (m, n) is ΔI_{mn} and the phase error is $\Delta\phi_{mn}$, where $\Delta\phi_{mn}$ is a smaller amount after being converted to the radian system. Then, the array factor of the array antenna becomes

$$\begin{aligned} AF = \sum_{m,n} I_{mn}\left(1 + \Delta\delta_{mn}\right)\exp\left\{jk\left[md_x\left(u - u_0\right)\right.\right. \\ \left.\left. + nd_y\left(v - v_0\right)\right]\right\}\exp\left(j\Delta\phi_{mn}\right). \end{aligned} \tag{8}$$

According to Taylor's expansion,

$$\exp\left(j\Delta\phi_{mn}\right) = 1 + j\Delta\phi_{mn} + (1 + j) * o\left(\Delta\phi_{mn}\right). \tag{9}$$

After finishing the expression of the antenna array factor, we can get

$$\begin{aligned} AF &= \sum_{m,n} I_{mn}\left(1 + \Delta\delta_{mn}\right)\exp\left\{jk\left[md_x\left(u - u_0\right) + nd_y\left(v - v_0\right)\right]\right\} * \left[1 + j\Delta\phi_{mn}\right], \\ &= \sum_{m,n} I_{mn}\exp\left\{jk\left[md_x\left(u - u_0\right) + nd_y\left(v - v_0\right)\right]\right\} + \sum_{m,n}\Delta\delta_{mn}\exp\left\{jk\left[md_x\left(u - u_0\right) + nd_y\left(v - v_0\right)\right]\right\} \\ &\quad + j\Delta\phi_{mn}\sum_{m,n} I_{mn}\exp\left\{jk\left[md_x\left(u - u_0\right) + nd_y\left(v - v_0\right)\right]\right\} \\ &\quad + j\Delta\phi_{mn}\sum_{m,n}\Delta\delta_{mn}\exp\left\{jk\left[md_x\left(u - u_0\right) + nd_y\left(v - v_0\right)\right]\right\} = AF_0 + \Delta AF_1 + \Delta AF_2 + \Delta AF_3. \end{aligned} \tag{10}$$

Among them, the elements are

$$\begin{aligned} \Delta AF_1 &= \sum_{m,n}\Delta\delta_{mn}AF_0, \\ \Delta AF_2 &= j\Delta\phi_{mn}AF_0, \\ \Delta AF_3 &= j\Delta\phi_{mn}\sum_{m,n}\Delta\delta_{mn}\exp\left\{jk\left[md_x\left(u - u_0\right) + nd_y\left(v - v_0\right)\right]\right\}. \end{aligned} \tag{11}$$

Since ΔAF_3 is the product of two minimal errors, it is ignored here. The array factor can be simplified as

$$AF = AF_0 + \Delta AF_1 + \Delta AF_2, \tag{12}$$

where AF_0 is the array factor of the two-dimensional array antenna under the ideal amplitude and phase distribution; ΔAF_1 is the amount of change caused by the amplitude error; and ΔAF_2 is the amount of change caused by the phase error.

$$E(\theta,\phi) = EP * AF = f(\theta,\phi) * AF. \tag{13}$$

The ideal power lobe function is

$$P_0 = E_0(u) * E_0^*(u). \tag{14}$$

Theoretically, the sidelobes of $E_0(u)$ and $P_0(u)$ can be designed to be arbitrarily low, but due to the existence of amplitude and phase errors, the reduction of the sidelobe level is limited. When there is amplitude and phase error between each unit, column and column, the lobe function is

$$\begin{aligned} E(\theta,\phi) = f(\theta,\phi)\sum_{m,n} I_{mn}\left(1 + \delta_{mn}\right)\exp\left(j\Delta\varphi_{mn}\right) \\ * \exp\left\{jk\left[md_x\left(u - u_0\right) + nd_y\left(v - v_0\right)\right]\right\}, \end{aligned} \tag{15}$$

where δ_{mn} and φ_{mn} are the amplitude and phase distributions of radiating element (m, n) in the antenna array. The amplitude and phase error can be expressed by Gaussian distribution, the mean value is 0, and the variance is δ_{mn}^2,

φ_{mn}^2. According to the central limit theorem, it can be proved that the sidelobe level R after considering the error obeys the Rician distribution; namely,

$$\begin{aligned} P(R) &= \frac{R}{\delta^2} = \exp\left(-\frac{R^2 + S_m}{2\delta^2}\right) * I_0\left(\frac{RS_m}{\delta^2}\right), \\ I_0(x) &= \frac{1}{2\pi}\int_{-\pi}^{\pi} e^{x\cos\varphi}\mathrm{d}\varphi, \\ \delta_E^2 &= \frac{\delta_{ae}^2 + \delta_{\varphi e}^2}{MN\eta}, \\ \eta &= \frac{\left(\sum\sum I_{mn}\right)^2}{MN\sum\sum I_{mn}^2}. \end{aligned} \tag{16}$$

I_0 is the zero-order modified Bessel function; S_m is the sidelobe level value under ideal conditions; $\delta^2 = \delta_E^2/2$, δ_E^2 is the variance of the lobe, which represents the degree of agreement between the actual lobe and the theoretical design band; and η characterizes the aperture efficiency of the array weight. Therefore, the probability that the sidelobe is lower than the given value RT is

$$\begin{aligned} P(R < RT) &= \int_0^{RT} P(R)\mathrm{d}R, \\ \text{limit sidelobe level} &\approx 11\,\mathrm{dB} + 101\,g\left(\frac{\delta_E^2}{2}\right). \end{aligned} \tag{17}$$

In practical applications, in order to facilitate the implementation of the project, according to the modular design requirements of the antenna array, the array is usually divided into multiple small subarrays or modules, which are cascaded through the feed network. In the cascading process, random errors are generated in units of subarrays. The following formula is the expression of the antenna pattern when the array is used as a subarray to construct the array. The division of other subarrays is similar:

$$\begin{aligned} E(\theta,\phi) &= f(\theta,\phi)\sum_n (1+\delta_n)\exp(j\Delta\varphi_n) \\ &\quad * \sum_m I_{mn}(1+\delta_{mn})\exp(j\Delta\varphi_{mn}) \\ &\quad \cdot \exp\left\{jk\left[md_x(u-u_0) + nd_y(v-v_0)\right]\right\}, \end{aligned} \tag{18}$$

where δ_n and φ_n are the amplitude and phase distribution of the nth column of radiating elements in the antenna array.

3.3. Structural Error. The structural error of the antenna array includes the processing error of the array, the installation error of the radiating element, the antenna frame and the subarray, and the structural deformation error caused by the deformation of the antenna. In the active phased array, processing, assembly, and other links will cause the deformation of the array and generate random errors. In the actual working environment, the factors such as vibration, impact, and high and low temperature will also cause the deformation of the planar array and finally change the position of the element to produce deformation errors, which will reduce the electromagnetic performance of the antenna [34]. As a result, the active phased array has raised sidelobes, decreased gain, and worsened pointing accuracy. Therefore, the study of the relationship between the coupling active phased array structure and electromagnetic analysis antenna electrical properties varies with structural changes in the error active phased bursts of the same size curve surface [35, 36], to obtain the critical value wavefront deformation and random error combined, can provide quantitative theoretical guidance for structural design and reasonable allocation of tolerances.

4. Simulation Analysis of Random Error in Amplitude and Phase

4.1. Random Error Simulation Analysis. The amplitude and phase errors in the simulation analysis process of amplitude and phase random errors are random values. The random error probability distribution obeys the Gaussian distribution, and the error value range is defined by the variance.

In the simulation process, taking a 16×16 planar phased array antenna as an example, the element spacing $\mathrm{d}x = 0.43\lambda$, $\mathrm{d}y = 0.52\lambda$, and the antenna element pattern uses Gaussian beams. In the process of random error analysis, the error source includes quantization error. The minimum quantization step size of the numerically controlled attenuator is 0.5 dB, and the digital phase shifter adopts a 6-phase shifter.

Let us take the random phase and amplitude errors with variances of $(0^\circ, 0\,\mathrm{dB}\backslash 0.3\,\mathrm{dB}\backslash 0.5\,\mathrm{dB}\backslash 1\,\mathrm{dB}\backslash 2\,\mathrm{dB})$ and $(10^\circ, 0\,\mathrm{dB}\backslash 0.3\,\mathrm{dB}\backslash 0.5\,\mathrm{dB}\backslash 1\,\mathrm{dB}\backslash 2\,\mathrm{dB})$ as an example to simulate the array pattern under the influence of random error. The simulation results of random amplitude and phase antenna without scanning and scanning -45° are shown in Figures 3 and 4. In the same way, the simulation result data under the conditions of $(5^\circ, 0\,\mathrm{dB}\backslash 0.3\,\mathrm{dB}\backslash 0.5\,\mathrm{dB}\backslash 1\,\mathrm{dB}\backslash 2\,\mathrm{dB})$ and $(20^\circ, 0\,\mathrm{dB}\backslash 0.3\,\mathrm{dB}\backslash 0.5\,\mathrm{dB}\backslash 1\,\mathrm{dB}\backslash 2\,\mathrm{dB})$ are plotted and analyzed with the above experimental data.

Table 1 shows the statistical results of technical indicators under the abovementioned random error conditions. Random errors have a significant impact on antenna gain, sidelobe level, and beam width and have little impact on beam pointing. As the error value increases, the antenna gain gradually decreases, the sidelobe level gradually increases, and the beam width gradually expands. When the error value is large, the beam direction will also change to a certain extent.

According to the simulation results in Table 1, under the influence of random errors, the gain, sidelobe level, etc., change, which affects the array antenna gain and overall performance. As the random error variance increases, the average sidelobe level and the first sidelobe level of the array pattern also increase. When the amplitude random error variance exceeds 0.5 dB and the

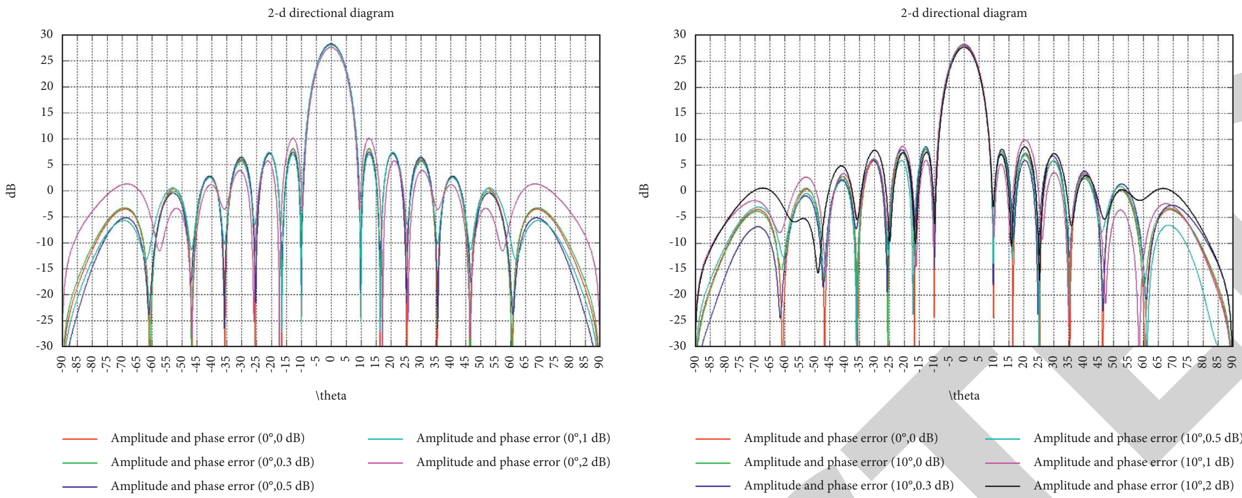

(a) (b)

Figure 3: Simulation results of random amplitude and phase antenna without scanning pattern: (a) phase is 0°; (b) phase is 10°.

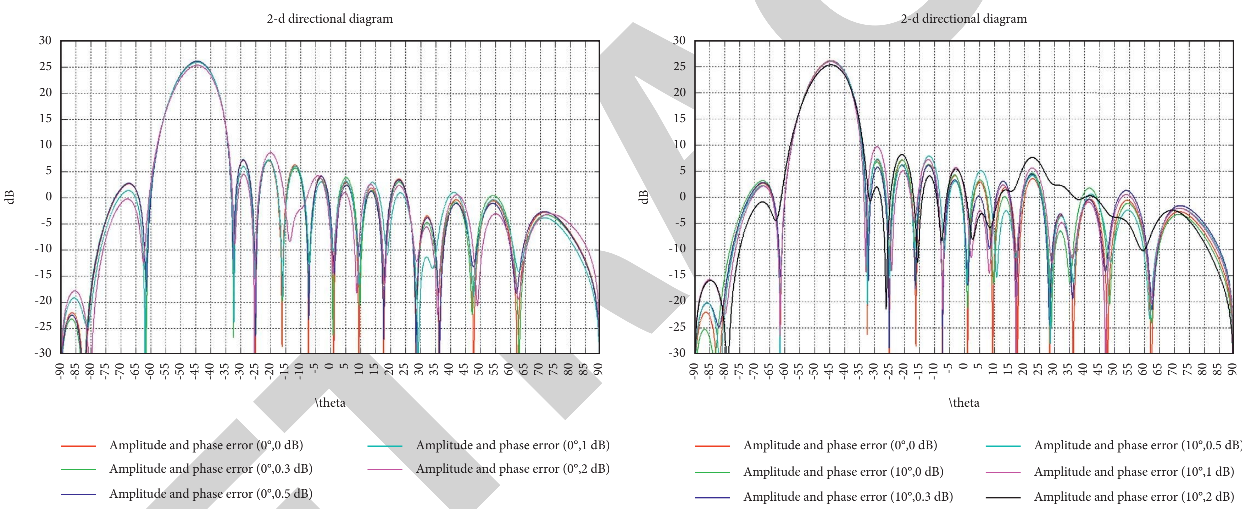

(a) (b)

Figure 4: Random amplitude and phase antenna scanning -45° pattern simulation results: (a) phase is 0°; (b) phase is 10°.

phase random error variance exceeds 10°, not only will the energy of the array pattern become more dispersed, the randomness of the sidelobe positions will increase, and the level of the first sidelobe will increase significantly compared to ideal conditions. In addition, the effect of random error on antenna beam scanning is like that when it is not scanning.

4.2. Verification of Multiple Random Results. The following is to verify the conclusion that the amplitude and phase random error is not greater than (0.5 dB, 10°). The simulation result of the antenna pattern with five random amplitude and phase errors is shown in Figure 5.

Table 2 counts the main technical indicators of antenna azimuth and elevation antennas with 5 different random errors. After comparison, the gain drop is less than or equal to 0.2 dB, the sidelobe level is less than or equal to 1 dB on average, the beam width changes up to 0.2°, and the influence of beam pointing is small.

5. Simulation Analysis of Structural Error

Figure 6 is a schematic diagram of a millimeter-wave antenna array and the center number of the array unit, where the x-axis is the azimuth direction, and the y-axis is the distance direction. The related data of the array is as follows:

(a) Working frequency: 24.25 GHz–27.5 GHz

(b) Model boundary size: 100 mm (azimuth direction) $*$ 112 mm (range direction)

(c) Rectangular array unit arrangement: 16 (azimuth direction) $*$ 16 (azimuth direction)

Table 1: Technical index statistics under the condition of random amplitude and phase error.

Random phase error (variance (°))	Scan angle	Random amplitude error (variance (dB))	Gain	Sidelobe level	3 dB beam width	Beam pointing
0	0	0	28.22	−20.25	8.00	0.00
		0.3	28.24	−19.61	8.00	0.00
		0.5	28.17	−20.77	8.00	0.00
		1	28.05	−20.22	8.00	0.00
		2	27.51	−17.92	8.20	0.00
	−45	0	26.08	−18.95	11.10	−44.40
		0.3	26.02	−18.56	11.20	−44.40
		0.5	25.94	−18.17	11.30	−44.40
		1	25.66	−17.56	11.40	−44.40
		2	25.66	−17.56	11.40	−44.40
5	0	0	28.20	−20.08	8.00	0.00
		0.3	28.18	−20.02	8.00	0.00
		0.5	28.17	−19.82	8.00	0.00
		1	28.02	−18.86	8.20	0.00
		2	27.70	−19.36	8.10	0.00
	−45	0	26.07	−18.55	11.20	−44.40
		0.3	26.04	−19.38	11.30	−44.40
		0.5	26.00	−18.82	11.30	−44.40
		1	25.98	−17.17	11.10	−44.40
		2	25.62	−17.03	11.00	−44.50
10	0	0	28.14	−20.04	8.00	−0.10
		0.3	28.13	−19.61	8.00	0.00
		0.5	28.08	−19.65	8.00	−0.10
		1	27.96	−18.14	8.10	0.00
		2	27.67	−19.18	7.90	0.00
	−45	0	26.00	−18.91	11.20	−44.50
		0.3	25.99	−19.92	11.20	−44.40
		0.5	25.98	−18.12	11.20	−44.40
		1	25.91	−16.27	11.10	−44.50
		2	25.30	−17.16	11.50	−44.40
20	0	0	27.84	−17.83	8.00	0.10
		0.3	27.90	−20.03	8.00	−0.10
		0.5	27.84	−17.77	8.10	0.10
		1	27.76	−16.42	8.00	0.00
		2	27.27	−19.62	8.00	0.10
	−45	0	25.80	−19.07	11.20	−44.50
		0.3	25.81	−18.87	11.20	−44.40
		0.5	25.72	−18.84	11.30	−44.40
		1	25.65	−17.19	11.10	−44.30
		2	25.27	−19.22	11.30	−44.30

(d) Antenna unit center spacing: 5 mm (azimuth direction) ∗ 6 mm (azimuth direction)

(e) Substrate material: Rogers 4350B. The thickness is 2.5 mm.

the radiating element. Here, 1.2 is selected, and the gain is about 6.4 dB. The position error of the left and right half arrays is simulated by MATLAB programming simulation, and the influence of the subarray error in the XY-direction on the antenna performance is analyzed.

5.1. Subarray Assembly Error. In the actual antenna design, $16 \times 8 = 128$ units are used as a subarray, and errors in the position of the subarray must be considered during the assembly process.

This paper takes 16×16 planar phased array antenna, that is, two subarrays, as an example. The element spacing is $dx = 0.43\lambda$, $dy = 0.52\lambda$, the antenna element pattern uses Gaussian beam, and the element pattern function is $EP = \cos(\theta)^{EF/2}$. Among them, EF determines the gain of the radiating element. Here, 1.2 is selected, and the gain is about 6.4 dB. The position error of the left and right half arrays is simulated by MATLAB programming simulation, and the influence of the subarray error in the XY-direction on the antenna performance is analyzed.

5.1.1. Subarray Error in the X-Direction. When there is an 0.2λ error in the X-direction of the left and right half of the array, the array element grid is shown in Figure 7. The experiment simulated the changes of the antenna pattern with an error value of 0: 0.05λ: 0.2λ.

Figure 8 shows the projection of the three-dimensional pattern in the UV space when there is a 0.2λ error in the left and right half of the antenna. Figure 9 shows the simulation results of the directional pattern of the antenna azimuth

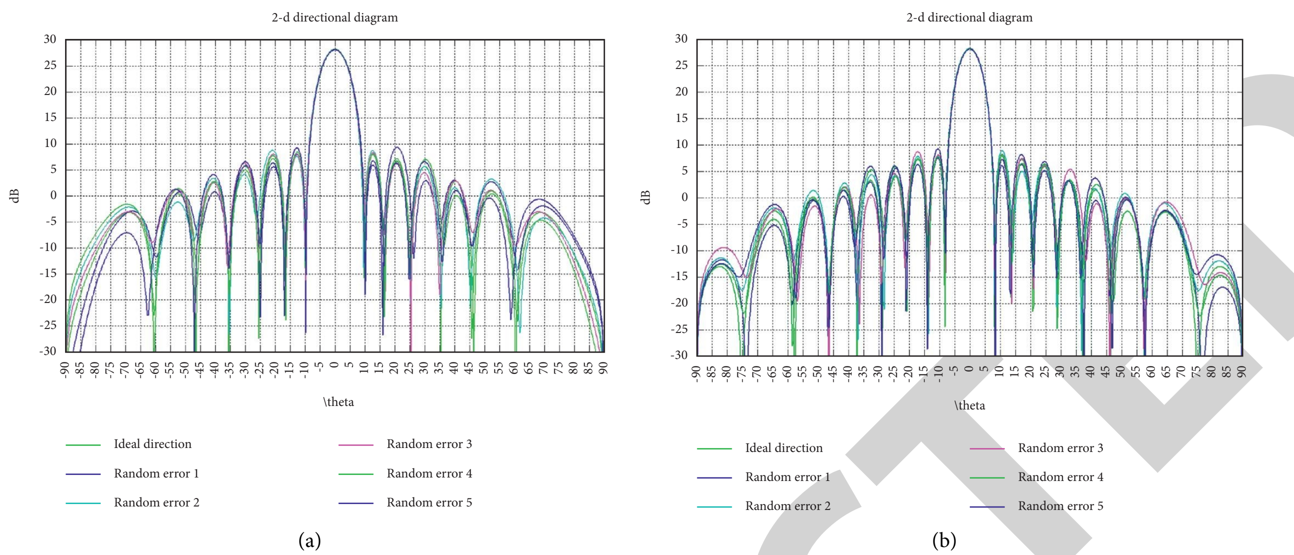

FIGURE 5: Simulation results of antenna pattern with five random amplitude and phase errors. (a) Azimuth plane. (b) Elevation plane.

TABLE 2: Five-order random amplitude and phase error antenna technical index statistics.

No.	Directional map section	Random times	Gain	Sidelobe level	3 dB beam width	Beam pointing
1	Azimuth plane	Ideal situation	28.22	−20.34	8.00	0.00
2		1	28.07	−18.76	7.80	0.00
3		2	28.13	−19.40	7.80	0.00
4		3	28.11	−19.84	8.00	0.00
5		4	28.12	−19.73	7.80	0.00
6		5	28.11	−18.89	8.00	0.00
7	Elevation plane	Ideal situation	28.22	−20.29	6.40	0.00
8		1	28.09	−20.56	6.60	0.00
9		2	28.15	−19.25	6.40	0.00
10		3	28.14	−19.44	6.60	0.00
11		4	28.12	−19.97	6.60	0.00
12		5	28.11	−18.88	6.60	0.00

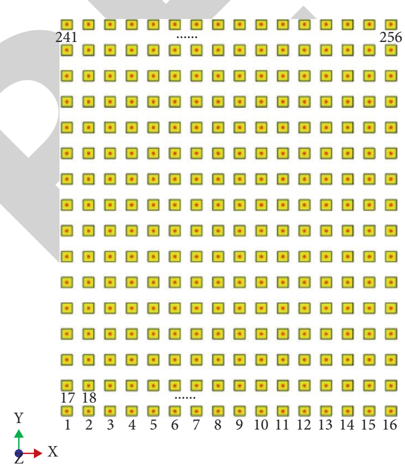

FIGURE 6: Schematic diagram of a millimeter-wave antenna array.

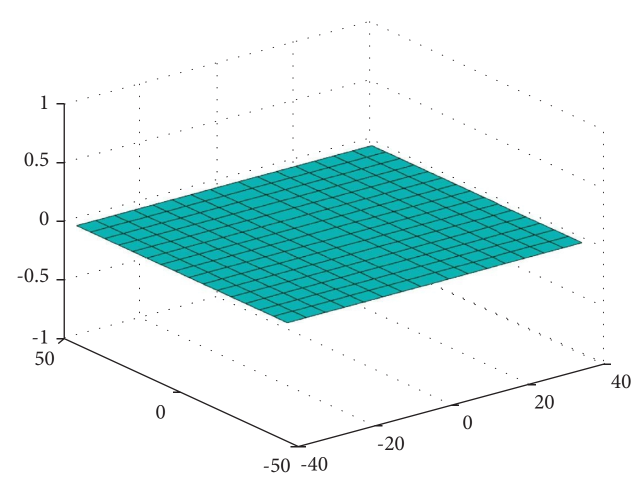

FIGURE 7: Position error of the left and right half arrays in the X-direction.

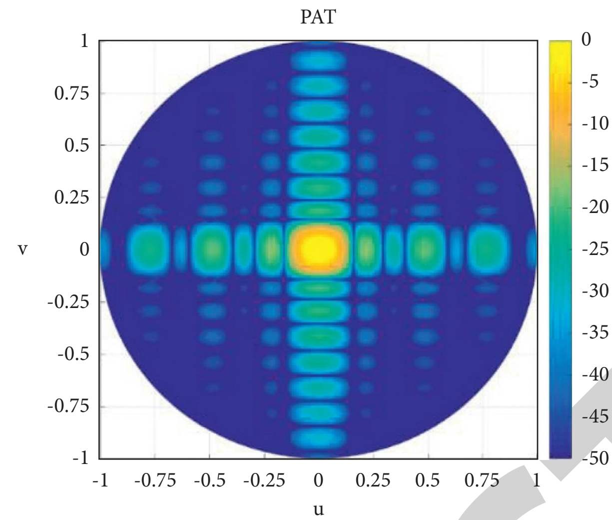

Figure 8: Change of the position error pattern of the left and right half arrays in the X-direction (0.2λ).

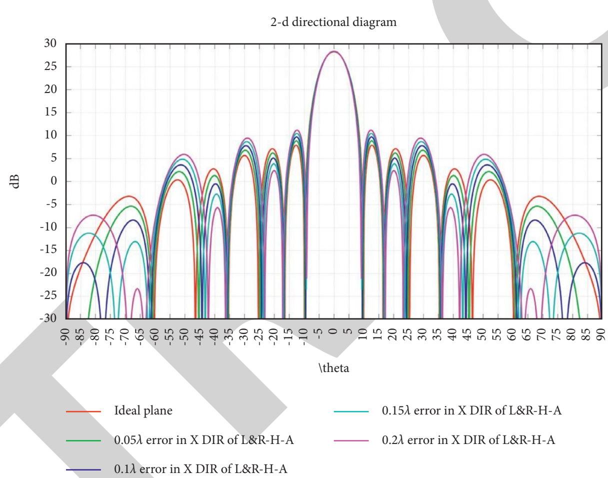

Figure 9: The change of the azimuth pattern caused by the position error of the left and right half arrays in the X-direction.

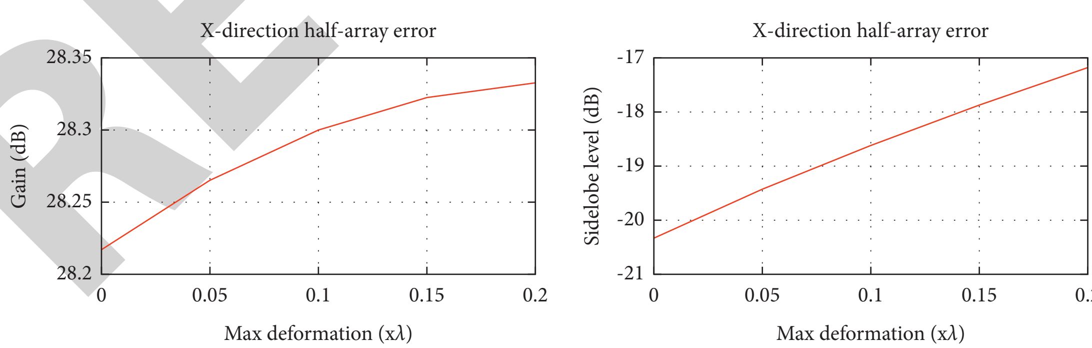

(a) (b)

Figure 10: Continued.

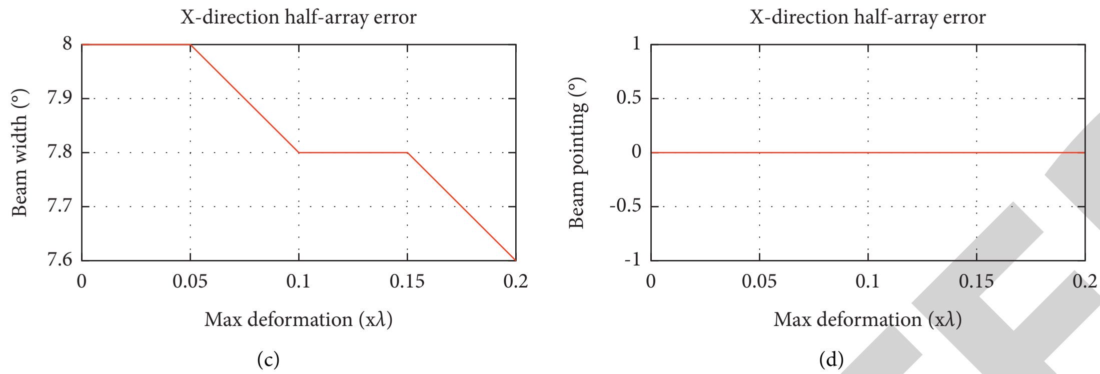

FIGURE 10: Changes in technical indicators caused by the position error of the left and right half arrays in the X-direction. (a) Gain. (b) Sidelobe level. (c) Beam width. (d) Beam pointing.

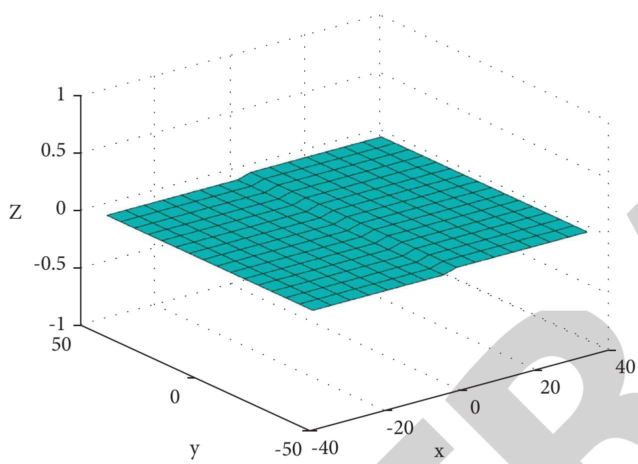

FIGURE 11: Position error of the left and right half arrays in the Y-direction.

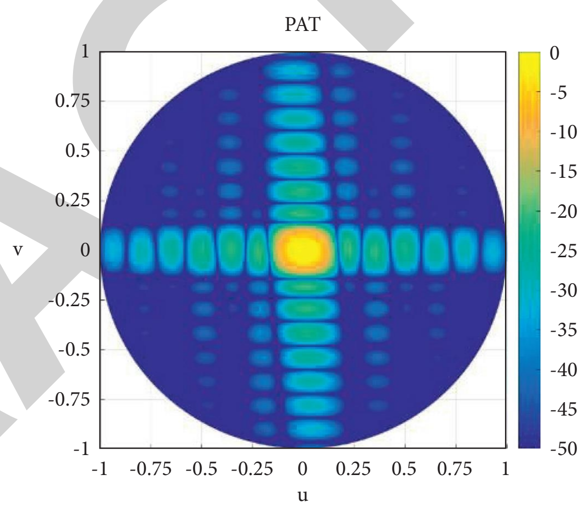

FIGURE 12: Change of the position error pattern of the left and right half arrays in the Y-direction (0.2λ).

plane when the left and right half arrays have different errors in the X-direction. The elevation plane has almost no effect. Figure 10 shows the changes in the technical indicators of the antenna azimuth plane when the left and right half arrays have different errors in the X-direction.

5.1.2. Subarray Error in the Y-Direction. When there is a 0.2λ error in the Y-direction of the left and right half of the array, the array element grid is shown in Figure 11. The experiment simulated the changes of the antenna pattern with an error value of 0: 0.05λ: 0.2λ.

Figure 12 shows the projection of the three-dimensional pattern in the UV space when there is a 0.2λ error in the left and right half of the antenna. Figure 13 shows the simulation results of the antenna elevation plane pattern when the left and right half arrays have different errors in the Y-direction. The azimuth plane has little influence. Figure 14 shows the changes in the technical indicators of the antenna azimuth plane when the left and right half arrays have different errors in the Y-direction.

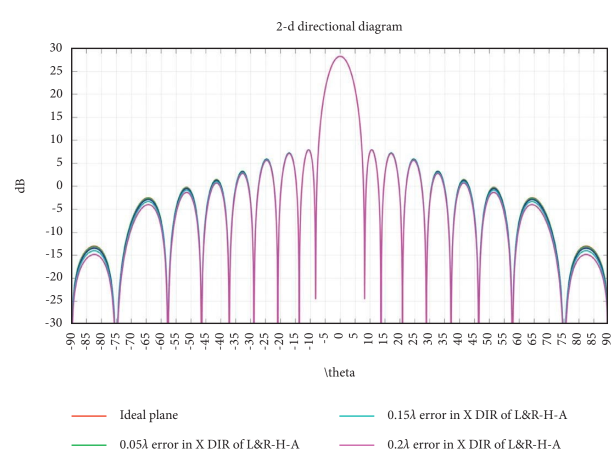

FIGURE 13: Change of the azimuth pattern caused by the position error of the left and right half arrays in the Y-direction.

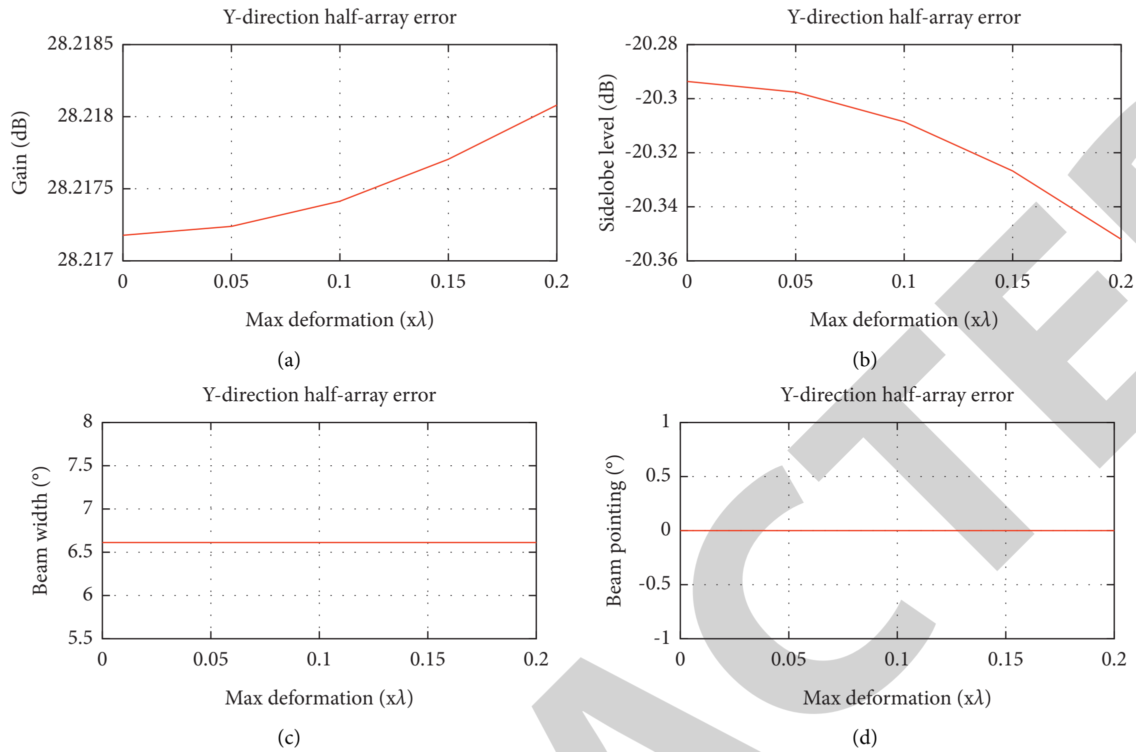

Figure 14: Changes in technical indicators caused by the position error of the left and right half arrays in the Y-direction. (a) Gain. (b) Sidelobe level. (c) Beam width. (d) Beam pointing.

5.1.3. Subarray Error in XY-Direction. Figure 15 shows the projection of the three-dimensional pattern in the UV space when there is a 0.1λ error in the left and right half of the antenna.

Table 3 shows the statistics of technical indicators such as antenna gain and sidelobe level when the XY-directions change at the same time.

From the above simulation results, it can be concluded that the gaps produced by the left and right half arrays in the X-direction will affect the distribution of antenna radiation power in space, and the impact on the sidelobe level is more obvious. As the gap increases, the electrical aperture of the planar array becomes larger, the gain becomes larger, the beam width becomes narrower, and the beam direction does not change. The gaps produced by the left and right half arrays in the Y direction will affect the distribution of antenna radiation power in space, causing tilt rotation, which has a significant impact on the far-area sidelobe level. As the gap increases, the electrical aperture of the planar array becomes larger, the gain becomes larger, the beam width becomes narrower, and the beam direction does not change. When the XY-direction changes at the same time, it is a combination of the above two situations.

In practical applications, according to the principle that the sidelobe level deterioration is not greater than 1 dB, the error in the X-direction should be $\leq 0.05\lambda$, and the error in the Y-direction should be $\leq 0.1\lambda$.

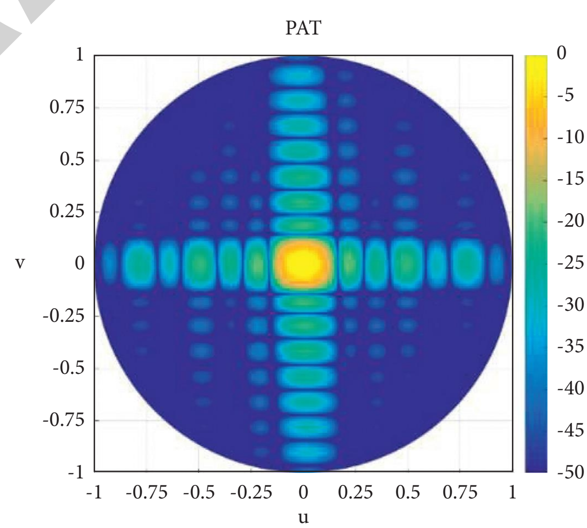

Figure 15: Position error pattern changes of the left and right half arrays in the XY-direction (0.1λ).

5.2. Subarray Deformation Error. Assuming that a vibration load is applied during the operation of the radar, under the constraints of the four corners, the antenna array will undergo symmetrical and asymmetrical deformation. For the planar rectangular active phased array antenna, the deformation of its subarray is usually saddle-shaped deformation.

Table 3: XY-direction changes at the same time technical indicator statistics.

No.	Directional map section	X-axis	Y-axis	Gain	Sidelobe level	3 dB beamwidth	Beam pointing
1			0	28.22	−20.33	8	0
2		0	0.05	28.22	−20.33	8	0
3			0.1	28.22	−20.33	8	0
4			0	28.26	−19.43	8	0
5	Azimuth plane	0.05	0.05	28.26	−19.43	8	0
6			0.1	28.26	−19.43	8	0
7			0	28.30	−18.62	7.8	0
8		0.1	0.05	28.30	−18.62	7.8	0
9			0.1	28.30	−18.62	7.8	0
10			0	28.22	−20.29	6.6	0
11		0	0.05	28.22	−20.30	6.6	0
12			0.1	28.22	−20.31	6.6	0
13			0	28.26	−20.29	6.6	0
14	Elevation plane	0.05	0.05	28.26	−20.30	6.6	0
15			0.1	28.26	−20.31	6.6	0
16			0	28.30	−20.29	6.6	0
17		0.1	0.05	28.30	−20.30	6.6	0
18			0.1	28.30	−20.31	6.6	0

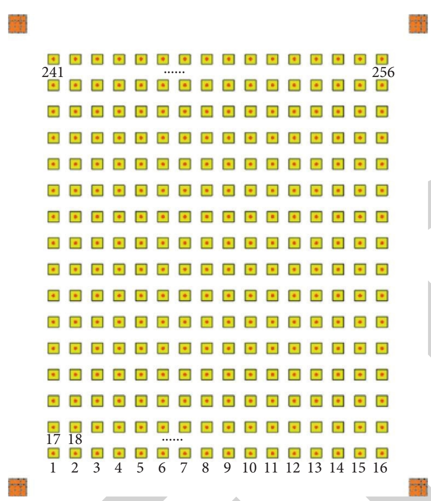

Figure 16: Matrix constraint condition.

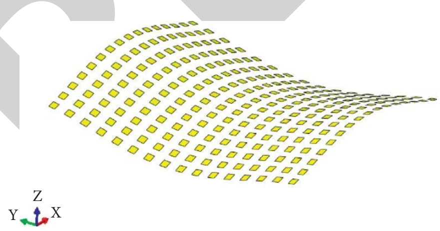

Figure 17: Saddle deformation.

The constraints are shown in Figure 16. A typical saddle-shaped deformation is listed below, the effect of antenna deformation on the antenna pattern is simulated and analyzed, and the main technical indicators of the antenna are counted.

Table 4: Normalized deformation data at the center of the antenna element.

Unit no.	Normalized data
1	0.0559
2	0.21
3	0.384
4	0.56
5	0.722
6	0.855
7	0.951
8	1
9	1
10	0.951
11	0.855
12	0.722
13	0.56
14	0.384
15	0.21
16	0.0559
17	−0.065
18	0.0901
19	0.257
20	0.423
21	0.575
22	0.701
23	0.791
24	0.837
25	0.837
26	0.791
27	0.701
28	0.575
29	0.423
30	0.257
31	0.0901
32	−0.065
33	−0.217
34	−0.0543
35	0.113
36	0.275
37	0.422

Table 4: Continued.

Unit no.	Normalized data
38	0.543
39	0.629
40	0.673
41	0.673
42	0.629
43	0.543
44	0.422
45	0.275
46	0.113
47	−0.0543
48	−0.217
49	−0.381
50	−0.209
51	−0.0381
52	0.124
53	0.269
54	0.388
55	0.472
56	0.515
57	0.515
58	0.472
59	0.388
60	0.269
61	0.124
62	−0.0381
63	−0.209
64	−0.381
65	−0.538
66	−0.358
67	−0.182
68	−0.0176
69	0.128
70	0.245
71	0.328
72	0.371
73	0.371
74	0.328
75	0.245
76	0.128
77	−0.0176
78	−0.182
79	−0.358
80	−0.538
81	−0.672
82	−0.485
83	−0.305
84	−0.138
85	0.0083
86	0.126
87	0.209
88	0.251
89	0.251
90	0.209
91	0.126
92	0.0083
93	−0.138
94	−0.305
95	−0.485
96	−0.672
97	−0.769

Table 4: Continued.

Unit no.	Normalized data
98	−0.578
99	−0.395
100	−0.225
101	−0.0781
102	0.0402
103	0.123
104	0.166
105	0.166
106	0.123
107	0.0402
108	−0.0781
109	−0.225
110	−0.395
111	−0.578
112	−0.769
113	−0.821
114	−0.627
115	−0.442
116	−0.271
117	−0.123
118	−0.0048
119	0.0781
120	0.121
121	0.121
122	0.0781
123	−0.0048
124	−0.123
125	−0.271
126	−0.442
127	−0.627
128	−0.821
129	−0.821
130	−0.627
131	−0.442
132	−0.271
133	−0.123
134	−0.0048
135	0.0781
136	0.121
137	0.121
138	0.0781
139	−0.0048
140	−0.123
141	−0.271
142	−0.442
143	−0.627
144	−0.821
145	−0.769
146	−0.578
147	−0.395
148	−0.225
149	−0.0781
150	0.0402
151	0.123
152	0.166
153	0.166
154	0.123
155	0.0402
156	−0.0781
157	−0.225

Table 4: Continued.

Unit no.	Normalized data
158	−0.395
159	−0.578
160	−0.769
161	−0.672
162	−0.485
163	−0.305
164	−0.138
165	0.0083
166	0.126
167	0.209
168	0.251
169	0.251
170	0.209
171	0.126
172	0.0083
173	−0.138
174	−0.305
175	−0.485
176	−0.672
177	−0.538
178	−0.358
179	−0.182
180	−0.0176
181	0.128
182	0.245
183	0.328
184	0.371
185	0.371
186	0.328
187	0.245
188	0.128
189	−0.0176
190	−0.182
191	−0.358
192	−0.538
193	−0.381
194	−0.209
195	−0.0381
196	0.124
197	0.269
198	0.388
199	0.472
200	0.515
201	0.515
202	0.472
203	0.388
204	0.269
205	0.124
206	−0.0381
207	−0.209
208	−0.381
209	−0.217
210	−0.0543
211	0.113
212	0.275
213	0.422
214	0.543
215	0.629
216	0.673
217	0.673
218	0.629
219	0.543
220	0.422
221	0.275
222	0.113
223	−0.0543
224	−0.217
225	−0.065
226	0.0901
227	0.257
228	0.423
229	0.575
230	0.701
231	0.791
232	0.837
233	0.837
234	0.791
235	0.701
236	0.575
237	0.423
238	0.257
239	0.0901
240	−0.065
241	0.0559
242	0.21
243	0.384
244	0.56
245	0.722
246	0.855
247	0.951
248	1
249	1
250	0.951
251	0.855
252	0.722
253	0.56
254	0.384
255	0.21
256	0.0559

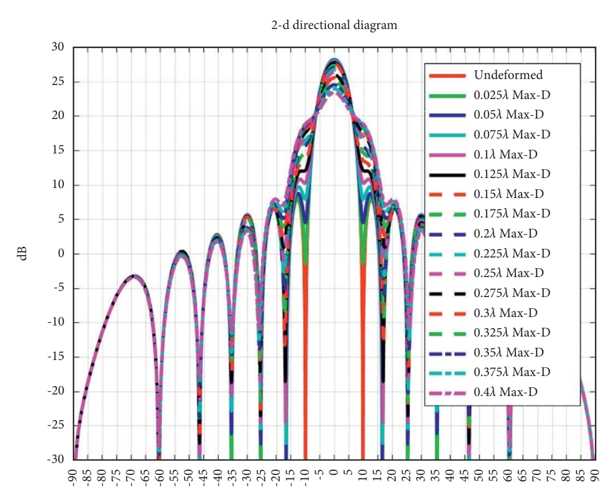

Figure 18: Azimuth plane of saddle-shaped deformation.

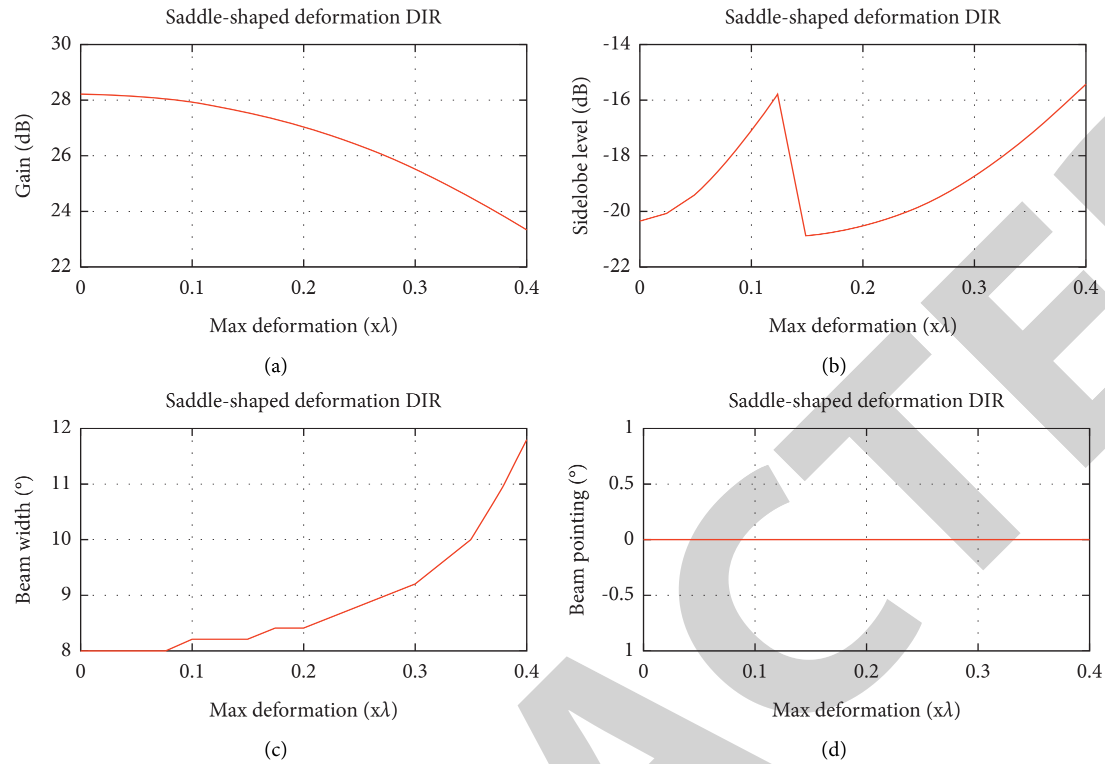

FIGURE 19: Changes in technical indicators of azimuth plane caused by saddle-shaped deformation. (a) Gain. (b) Sidelobe level. (c) Beam width. (d) Beam pointing.

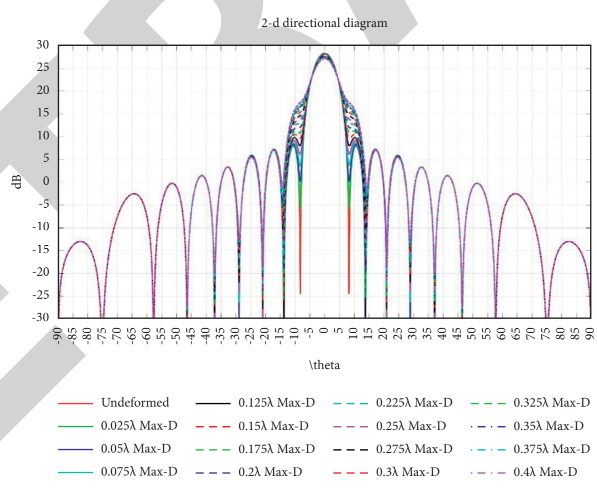

FIGURE 20: Elevation plane of saddle-shaped deformation.

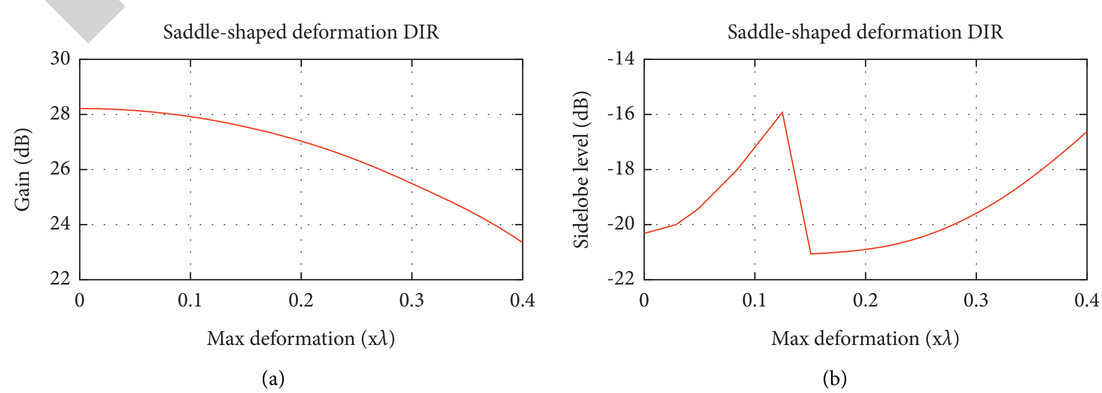

FIGURE 21: Continued.

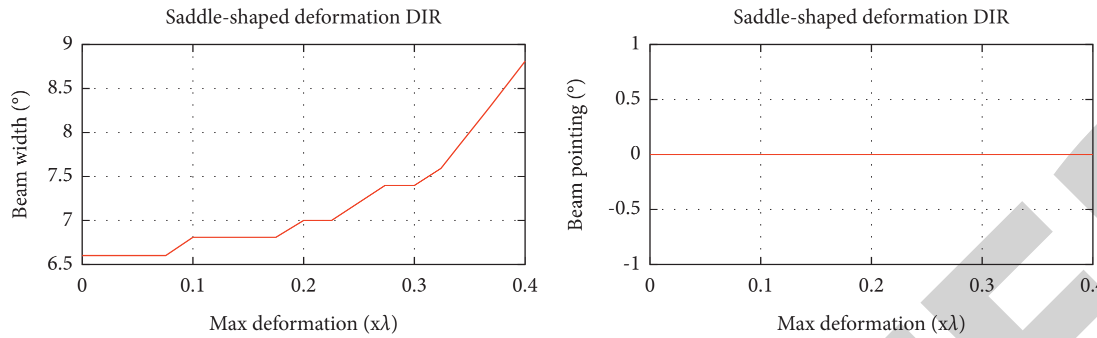

(c) (d)

Figure 21: Changes in technical indicators of elevation plane caused by saddle-shaped deformation. (a) Gain. (b) Sidelobe level. (c) Beam width. (d) Beam pointing.

Table 5: Statistics of saddle-shaped deformation technical indicators.

No.	Directional map section	Max deformation	Gain	Sidelobe level	3 dB beam width	Beam pointing
1		0	28.22	−20.33	8.00	0.00
2		0.025	28.20	−20.09	8.00	0.00
3		0.05	28.14	−19.40	8.00	0.00
4		0.075	28.05	−18.37	8.00	0.00
5		0.1	27.92	−17.12	8.20	0.00
6		0.125	27.75	−15.73	8.20	0.00
7		0.15	27.55	−20.90	8.20	0.00
8		0.175	27.31	−20.75	8.40	0.00
9	Azimuth plane	0.2	27.02	−20.54	8.40	0.00
10		0.225	26.71	−20.24	8.60	0.00
11		0.25	26.35	−19.86	8.80	0.00
12		0.275	25.95	−19.37	9.00	0.00
13		0.3	25.51	−18.78	9.20	0.00
14		0.325	25.04	−18.09	9.60	0.00
15		0.35	24.52	−17.30	10.00	0.00
16		0.375	23.96	−16.43	10.80	0.00
17		0.4	23.37	−15.47	11.80	0.00
18		0	28.22	−20.29	6.60	0.00
19		0.025	28.20	−20.06	6.60	0.00
20		0.05	28.14	−19.39	6.60	0.00
21		0.075	28.05	−18.40	6.60	0.00
22		0.1	27.92	−17.21	6.80	0.00
23		0.125	27.75	−15.91	6.80	0.00
24		0.15	27.55	−21.05	6.80	0.00
25		0.175	27.31	−20.99	6.80	0.00
26	Elevation plane	0.2	27.02	−20.89	7.00	0.00
27		0.225	26.71	−20.71	7.00	0.00
28		0.25	26.35	−20.44	7.20	0.00
29		0.275	25.95	−20.07	7.40	0.00
30		0.3	25.51	−19.59	7.40	0.00
31		0.325	25.04	−18.99	7.60	0.00
32		0.35	24.52	−18.29	8.00	0.00
33		0.375	23.96	−17.49	8.40	0.00
34		0.4	23.37	−16.61	8.80	0.00

5.2.1. Saddle-Shaped Deformation of Arrays. Figure 17 shows the saddle-shaped deformation of the antenna array. The normalized deformation data of the center of each antenna element is shown in Table 4.

Based on the normalized deformation, the maximum deformation of the antenna array was set, and the azimuth and elevation patterns of the antenna were simulated when the maximum deformation became 0: 0.025λ: 0.4λ. Figure 18 shows the changes in the pattern of the array azimuth plane under saddle-shaped deformation. Figure 19 shows the changes in the main technical indicators of the array azimuth under saddle-shaped deformation. Figure 20 shows

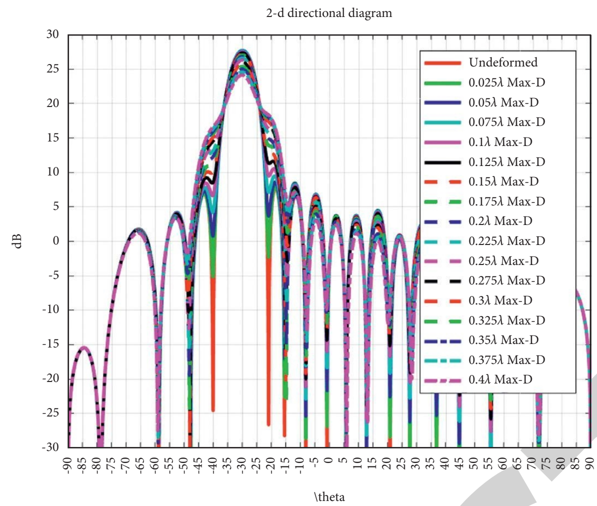

FIGURE 22: Saddle-shaped deformation azimuth scanning −30° direction map.

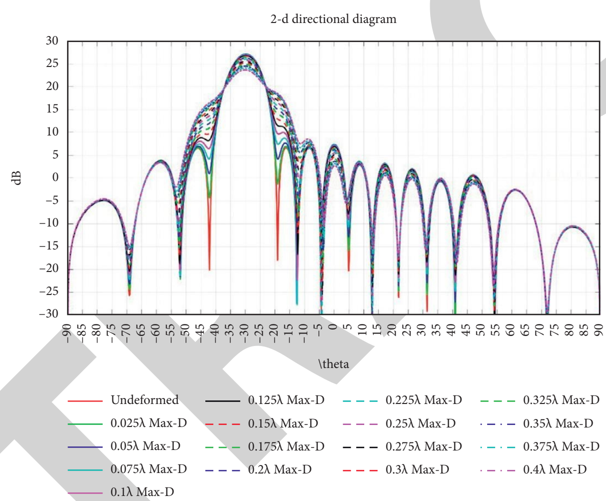

FIGURE 23: Saddle-shaped deformation elevation scanning −30° direction map.

the changes in the pattern of the array elevation plane under saddle-shaped deformation. Figure 21 shows the changes in the main technical indicators of the array elevation plane under saddle-shaped deformation. Table 5 shows the changes in the main technical indicators of the antenna under the saddle-shaped deformation of the array.

From Figures 18–21 and Table 5, the saddle-shaped deformation has a great influence on the azimuth plane and the elevation plane pattern of the planar array. As the amount of deformation increases, the antenna gain gradually decreases, the sidelobe level gradually increases, and the beam width gradually expands, which has almost no effect on the antenna beam direction. When the deformation amount is greater than or equal to 0.15λ, the azimuth plane and the elevation plane pattern begin to defocus, the pattern is no longer focused, and the first zero point disappears.

5.2.2. Analysis of Deformation Error Impact. In order to verify whether the saddle-shaped deformation will affect the scanning beam of the antenna, the azimuth plane and the elevation plane, respectively, scan the directional patterns of −30° under different maximum deformation variables, as shown in Figures 22 and 23. It can be seen from the figure that the influence of saddle-shaped deformation on antenna beam scanning is basically the same as when the antenna is not scanning.

Integrating the technical indicators of the azimuth plane and the elevation plane, the maximum deformation error of the saddle-shaped deformation is $\leq 0.05\lambda$ and the deterioration of the technical indicators is acceptable. In engineering practice, the maximum deformation error value should be controlled to be $\leq 0.05\lambda$.

6. Conclusions

Taking a 16×16 two-dimensional array antenna as an example, this paper constructed a millimeter-wave antenna array error theoretical model. The influence of random errors caused by production, XY-direction errors caused by assembly, and saddle-shaped deformation of the front on the electrical performance of the antenna under the condition that the size of the front is unchanged is analyzed. Through a large amount of data calculation, we have given the quantitative relationship between the influence of the error and the electrical performance of the antenna, drawn the influence relationship curve, and finally obtained the critical value. Engineers can refer to the analysis methods and conclusions in the article to estimate the antenna performance and put forward reasonable requirements for the processing tolerance of the antenna array within the allowable range of electrical performance. In follow-up research, we will further analyze the impact of other forms of errors on the electrical performance of the antenna and find the best correction method so that engineers can get a more optimized antenna design and assembly plan. The specific indicators obtained from the experiment are as follows:

(1) In engineering practice, we should try to eliminate the possible factors that produce random errors. At the same time, strictly control the production process and flow during the production and development process, so that the variance of the random phase and amplitude error does not exceed $(10^{\circ}, 0.5\,\mathrm{dB})$, to ensure a small impact on the array antenna pattern and meet the performance requirements of the array antenna.

(2) The errors caused by the assembly of the left and right half arrays, the gaps in the X-direction, have a more obvious impact on the sidelobe level, and the gaps in the Y-direction will affect the distribution of antenna radiation power in space, causing tilt rotation. When the XY-direction changes at the same time, it is a combination of the two situations. According to the sidelobe level deterioration being not more than 1 dB, the error in the X-direction should be $\leq 0.05\lambda$, and the error in the Y-direction should be $\leq 0.1\lambda$.

(3) Symmetrical deformations such as saddle-shaped deformations mainly affect the gain and energy distribution of the antenna and will not affect the beam direction. In engineering practice, to ensure that the sidelobe level deterioration is better than 1 dB, the maximum deformation should be better than 0.05λ.

Data Availability

All data, models, and codes generated or used during the study are included within this article.

Conflicts of Interest

The authors declare that they have no conflicts of interest regarding the publication of this paper.

Acknowledgments

This work was supported by the National Defense Basic Scientific Research Program of China under Grants JCKY2019210B005, JCKY2018204B025, and JCKY2017204B011, the Key Scientific Project Program of National Defense of China under Grant ZQ2019D20401, and the Open Program of National Engineering Laboratory for Modeling and Emulation in E-Government under Grant MEL-20-02, and the Foundation Strengthening Project of China under Grant no. 2019JCJZZD13300.

References

[1] J. Ou, J. Zhang, and R. Zhan, "Processing technology based on radar signal design and classification," *International Journal of Aerospace Engineering*, vol. 2020, Article ID 4673763, 19 pages, 2020.

[2] F. Zhang, *Research and Analysis of Millimeter-Wave Phased Array Antenna Array*, Nanjing University of Science and Technology, Nanjing, China, 2009.

[3] G. Federico, D. Caratelli, G. Theis, and A. B. Smolders, "A review of antenna array technologies for point-to-point and point-to-multipoint wireless communications at millimeter-wave frequencies," *International Journal of Antennas and Propagation*, vol. 2021, Article ID 5559765, 18 pages, 2021.

[4] H. Wang, L. Xu, Z. Yan, and T. A. Gulliver, "Low-complexity MIMO-FBMC sparse channel parameter estimation for industrial big data communications," *IEEE Transactions on Industrial Informatics*, vol. 17, no. 5, pp. 3422–3430, 2021.

[5] L. Wan, K. Liu, Y.-C. Liang, and T. Zhu, "DOA and polarization estimation for non-circular signals in 3-D millimeter wave polarized massive MIMO systems," *IEEE Transactions on Wireless Communications*, vol. 20, no. 5, pp. 3152–3167, 2021.

[6] J. Shi, F. Wen, and T. Liu, "Nested MIMO radar: coarrays, tensor modeling, and angle estimation," *IEEE Transactions on Aerospace and Electronic Systems*, vol. 57, no. 1, pp. 573–585, 2021.

[7] X. Wang, M. Huang, and L. Wan, "Joint 2D-DOD and 2D-DOA estimation for coprime EMVS-MIMO radar," *Circuits, Systems, and Signal Processing*, vol. 40, no. 6, pp. 2950–2966, 2021.

[8] F. Wen, J. Shi, and Z. Zhang, "Closed-form estimation algorithm for EMVS-MIMO radar with arbitrary sensor geometry," *Signal Processing*, vol. 186, Article ID 108117, 2021.

[9] X. Yu, "Functional characteristics and application analysis of phased array radar," *China New Telecommunications*, vol. 21, no. 6, p. 168, 2019.

[10] J. He, L. Li, and T. Shu, "Sparse nested arrays with spatially spread orthogonal dipoles: high accuracy passive direction finding with less mutual coupling," *IEEE Transactions on Aerospace and Electronic Systems*, vol. 57, no. 4, pp. 2337–2345, 2021.

[11] C. Luison, A. Landini, P. Angeletti et al., "Aperiodic arrays for spaceborne SAR applications," *IEEE Transactions on Antennas and Propagation*, vol. 60, no. 5, pp. 2285–2294, 2012.

[12] D. Vollbracht, "Optimum phase excitations and probe- feed positions inside antenna arrays for the reduction of cross polarization radiation in demanding phased array weather radar applications," in *Proceedings of the 2016 10th European Conference on Antennas and Propagation (EuCAP)*, pp. 1–5, Davos, Switzerland, April 2016.

[13] S. K. Sharma, "Design and development of some novel phased arrays and anti-jamming antennas," in *Proceedings of the 2017 IEEE Radio and Antenna Days of the Indian Ocean (RADIO)*, p. 1, Cape Town, South Africa, September 2017.

[14] K. Wu, Y. Yao, X. Cheng, J. Yu, and X. Chen, "Design of high efficiency linearly polarized 8 × 8 millimeter-wave antenna

array," in *Proceedings of the 2019 IEEE Asia-Pacific Microwave Conference (APMC)*, pp. 735–737, Singapore, December 2019.

[15] J. A. Ortiz, N. Aboserwal, and J. L. Salazar, "A new analytical model based on diffraction theory for predicting cross-polar patterns of antenna elements in a finite phased array," in *Proceedings of the 2019 IEEE International Symposium on Phased Array System & Technology (PAST)*, pp. 1–4, Waltham, MA, USA, October 2019.

[16] D. Busuioc and S. Safavi-Naeini, "Low-cost antenna array and phased array architectures-design concepts and prototypes," in *Proceedings of the 2010 IEEE International Symposium on Phased Array Systems and Technology*, pp. 965–968, Waltham, MA, USA, October 2010.

[17] R. Mayo and S. Harmer, "A cost-effective modular phased array," in *Proceedings of the 2013 IEEE International Symposium on Phased Array Systems and Technology*, pp. 93–96, Waltham, MA, USA, October 2013.

[18] Y. Zhang, D. Ni Zhao, Q. Wang, Z. Long, and X. Shen, "Tolerance analysis of antenna array pattern and array synthesis in the presence of excitation errors," *International Journal of Antennas and Propagation*, vol. 2017, Article ID 3424536, 6 pages, 2017.

[19] G. Fang, X. Wang, and B. Gao, "The influence of position error and phase error on modular antenna array," *Modern Radar*, vol. 29, no. 12, pp. 83–89, 2007.

[20] H. S. C. Wang, "Performance of phased-array antennas with mechanical errors," *IEEE Transactions on Aerospace and Electronic Systems*, vol. 28, no. 2, pp. 535–545, 1992.

[21] J. Chen and Y. Zhou, "Analysis of thermal deformation error of spaceborne SAR phased array antenna," *Journal of Beijing University of Aeronautics and Astronautics*, vol. 30, no. 9, pp. 839–843, 2004.

[22] X. Zhang, "The influence of structure error on the electrical performance of antenna array," *Modern Navigation*, vol. 9, no. 5, pp. 357–361, 2018.

[23] A. Farina and L. Timmoneri, "Phased array systems for air, land and naval defence applications in Selex ES," in *Proceedings of the 8th European Conference on Antennas and Propagation (EU CAP)*, Hague, Netherlands, April 2014.

[24] S. J. Wijnholds, W. A. van Cappellen, J. G. bij de Vaate, and A. van Ardenne, "Phased-array antenna system development for radio-astronomy applications [Antenna Applications Corner," *IEEE Antennas and Propagation Magazine*, vol. 55, no. 6, pp. 293–308, 2013.

[25] A. Bar-Cohen and J. Albrecht, "Thermal management of active electronically scanned arrays," in *Proceedings of the IEEE International Symposium on Phased Array Systems & Technology*, Waltham, MA, USA, October 2013.

[26] G. Xia, Y. Fang, and W. Zhao, "Monitoring design of phased array radar transmitter based on PIC microcontroller serial polling communication," *Science and Technology Innovation Herald*, vol. 13, no. 17, pp. 74-75, 2016.

[27] Ge Zhao, J. Hu, and J. Zhang, "Gesture sensitivity analysis for high range resolution profile of midcourse target," *Radio Engineering*, vol. 42, no. 7, pp. 20–22, 2012.

[28] H. Fan and J. Yan, "The development status and prospects of phased array guidance technology," *Acta Aeronautica ET Astronautica Sinica*, vol. 36, no. 9, pp. 2807–2814, 2015.

[29] R. J. Mailloux, *Phased Array Antenna Handbook*, Artech House, Norwood, MA, USA, 3rd edition, 1994.

[30] Y. Chen and Y. Lu, "Performance analysis for millimetre wave array antenna systems based on influence of amplitude quantization error," in *Proceedings of the 2021 IEEE 6th International Conference on Computer and Communication Systems (ICCCS)*, Las Vegas, NV, USA, October 2021.

[31] T. Lindgren and J. Borg, "A measurement system for the position and phase errors of the elements in an antenna array subject to mutual coupling," *International Journal of Antennas and Propagation*, vol. 2012, Article ID 526121, 8 pages, 2012.

[32] Z. Xiong, "Research on the influence of amplitude and phase error on the performance of phased array antenna," *Doctoral dissertation, China Ship Research Institute, Shanghai, China*, 2012.

[33] C. Wang, M. Kang, W. Wang, and T. Pu, "Analysis of influence of structural deformation on electrical performance of phased array antenna," *Journal of Systems Engineering and Electronics*, vol. 35, no. 8, pp. 1644–1649, 2013.

[34] M. Kang, C. Wang, Y. Wang, W. Wang, and Q. Tu, "Analysis of influence of array plane error on performances of hexagonal Phased array antennas," in *Proceedings of the RSI General Assembly and Scientific Symposium*, Beijing, China, August 2014.

[35] T. Huang, Y. Yu, and L. Yi, "Design of highly isolated compact antenna array for MIMO applications," *International Journal of Antennas and Propagation*, vol. 2014, Article ID 473063, 5 pages, 2014.

[36] C. S. Wang, B. Y. Duan, F. S. Zhang, and M. B. Zhu, "Coupled structural-electromagnetic-thermal modelling and analysis of active phased array antennas," *IET Microwaves, Antennas & Propagation*, vol. 4, no. 2, pp. 247–257, 2010.